Rate Constants for the Thermal Dissociation of N_2O and the $O(^3P) + N_2O$ Reaction

Stuart K. Ross,† James W. Sutherland,* Szu-Cherng Kuo, and R. Bruce Klemm*

Department of Applied Science, Brookhaven National Laboratory, Upton, New York 11973-5000

Received: August 8, 1996; In Final Form: November 6, 1996[⊗]

The thermal dissociation of N_2O in argon was investigated by monitoring the formation of $O(^3P)$ atoms in the reflected shock regime using atomic resonance absorption spectrophotometry (ARAS). The total density and $[N_2O]$ ranges were, $(2.6 \times 10^{18})-(5.4 \times 10^{18})$ molecules cm^{-3} and $(3.3 \times 10^{12})-(7.9 \times 10^{15})$ molecules cm^{-3}, respectively. Values for the bimolecular rate constant (131 points), derived under low-pressure limit conditions are given by the Arrhenius expression: $k_1(T) = (1.18 \pm 0.16) \times 10^{-9}$ exp[(−57820 ± 460 cal mol^{-1})/RT] cm^3 molecule^{-1} s^{-1} for the temperature range, $1195 \le T \le 2384$ K. These results extend the low-temperature range of ARAS measurements of k_1 by about 200 °C which is very significant in 1/T; and the value of the rate constant was extended by more than an order of magnitude. The present data were combined with previously published ARAS data to form a composite data set with a total of 278 points. Although systematic differences between the data of the various groups were discernible, all the data are well represented by the following Arrhenius equation: $k_1(T) = (9.52 \pm 1.07) \times 10^{-10}$ exp[(−57570 ± 390 cal mol^{-1})/RT] cm^3 molecule^{-1} s^{-1} for the temperature range, $1195 \le T \le 2494$ K). Uncertainties in the Arrhenius expression are given at the one standard deviation level and the mean deviation of the experimental data from that predicted by the expression is ±26%. These results are compared to those from previous experimental studies. The rate of the reaction of $O(^3P)$ with N_2O was investigated experimentally and by kinetic modeling, but only over a limited temperature range, $1200 \le T \le 1400$ K. Upper limit values of the overall rate constant for the $O(^3P) + N_2O$ reaction were estimated by a statistical technique. These values were about a factor of 10 lower (with an overall uncertainty of about a factor of three) than those calculated from the recommended Arrhenius expressions of Baulch *et al.* (1973), Hanson and Salimian (1984), and Tsang and Herron (1991).

Introduction

The thermal dissociation of N_2O is of continuing interest, both in experimental and theoretical chemistry, and in technological processes such as combustion in fluidized beds, combustion under fuel lean conditions, and propellant combustion.[1,2] Consequently, there have been numerous experimental[1−25] and theoretical[26−33] studies to establish the kinetics and the dynamics of this reaction. In addition, the kinetics of this system are discussed in several review articles.[34−36]

Early studies of this unimolecular reaction established that it proceeds *via* a spin-forbidden, nonadiabatic pathway to form $O(^3P)$ atoms in preference to the spin allowed, but more endothermic dissociation to form $O(^1D)$ atoms:

$$N_2O(^1\Sigma^+) + M \rightarrow N_2(^1\Sigma_g^+) + O(^3P) + M \qquad \Delta_r H_0^\circ = 39 \text{ kcal mol}^{-1} \quad \text{(R1)}$$

$$N_2O(^1\Sigma^+) + M \rightarrow N_2(^1\Sigma_g^+) + O(^1D) + M \qquad \Delta_r H_0^\circ = 84 \text{ kcal mol}^{-1} \quad \text{(R1a)}$$

Dissociation occurs as a result of collision induced vibrational excitation of the singlet ground state to a critical "energy level" from which intersystem crossing takes place to a triplet state, which is predissociative.[34]

Most of these investigations employed shock tubes together with various analytical techniques such as mass spectroscopy,[3−5] chemiluminescence,[6] gas chromatography,[7,8] laser schlieren,[9] UV−vis emission[10]−absorption,[11−15] IR emission,[2,16−17] and most recently, O-atom resonance absorption spectrophotometry (ARAS).[18−22] Other studies employed flow tube methods[1,2,23] along with analytical techniques such as FT-IR spectroscopy and oxygen electrochemical analysis. As shown in Table 1, there are significant differences in the bimolecular rate constant expressions found, particularly among the activation energy values, which range from about 48 to 62 kcal mol^{-1}. The non-ARAS results, in particular, show the widest variability in values for the apparent activation energy and for individual values of $k_1(T)$. In contrast, results from studies that employed the ARAS technique display reasonably close agreement, especially a narrow range in activation energies[18−22] with most values clustering around 61 kcal mol^{-1}.

In their theoretical study, Cheng and Yarkony[32] calculated the potential energy surfaces involved and provided critical information on the crossing surfaces linking the ground state singlet to the three possible triplet states. These authors further show that only the linear A″ triplet state is important with state to state crossing occurring at an energy level of about 58 kcal mol^{-1} above the ground state. This calculated energy level should relate to the high-pressure activation energy for reaction R1. If so, the value of 58 kcal mol^{-1} would appear to be somewhat small in relation to both the majority of the low-pressure ARAS results (≈61 kcal mol^{-1}) and to the recently published[15] value for the high-pressure limit, $E_a^\infty = 62.6$ kcal mol^{-1}.

Fall-off behavior and the asymptotic approach to the high-pressure limit is observed only at very high pressures.[37] Reported high-pressure studies are summarized in Table 2, which includes results from studies by Allen *et al.*,[2] Olschewski

* Authors to whom correspondence should be addressed.

† Visiting Research Associate, permanent address: Department of Chemistry, University of Aberdeen, Meston Walk, Aberdeen AB9 2UE, Scotland, U.K.

⊗ Abstract published in *Advance ACS Abstracts,* February 1, 1997.

S1089-5639(96)02416-4 CCC: $14.00

TABLE 1: Low-Pressure Rate Constant Expressions Determined by Shock Tube Techniques for $N_2O + M \rightarrow N_2 + O(^3P) + M$, M = Ar

temperature (K)	pressure (Torr)	A (cm^3 molecule^{-1} s^{-1})	E_a (kcal mol^{-1})	refs
		Rate Expressions Determined *via* ARAS		
1850−2500	1350	2.40×10^{-9}	61.206	Roth and Just[18b]
1519−2408		2.23×10^{-9}	62.040	Pamidimukkala *et al.*[19]
1450−2200	760−1350	2.40×10^{-9}	59.465	Frank and Just[20a]
1600−2500	760	1.66×10^{-9}	60.470	Fujii *et al.*[21a]
1540−2500		2.76×10^{-10}	52.542	Michael and Lim[22b] [a]
		Rate Expressions Determined *via* Other Diagnostic Techniques		
1500−2500	80−250	1.66×10^{-9}	60.999	Jost *et al.*[11]
1500−2500	1140−2.28×10^5	8.32×10^{-10}	57.998	Olschewski *et al.*[12]
1000−2000	30−200	8.32×10^{-10}	57.001	Borisov and Skachkov[13]
1000−3000		7.80×10^{-10}	58.000	Soloukhin[6]
1850−2536	60−74	4.90×10^{-10}	52.367	Baber and Dean[10]
2160−2500	2−75	8.32×10^{-10}	58.000	Dove *et al.*[9]
1950−2800	37−77	1.91×10^{-10}	48.639	Dean[15]
2100−3200	77−238	4.50×10^{-10}	54.016	Dean and Steiner[16]
1815−3365	304−380	2.36×10^{-10}	51.282	Monat *et al.*[24]
1700−2400	112−744	6.47×10^{-10}	57.365	Endo *et al.*[28]
1688−3113	228−4560	5.25×10^{-10}	55.834	Rohrig *et al.*[15]
1685−2560	1290−3500	6.15×10^{-10}	54.966	Sulzmann *et al.*[25]
1820−3170	186−435	7.30×10^{-10}	56.001	Zaslonko *et al.*[14]
		Rate Expressions Recommended in Review Articles		
1300−2500		8.30×10^{-10}	57.623	Baulch *et al.*[34]
1500−2500		5.61×10^{-10}	56.761	Hanson and Salimian[35] [b]
1000−2500		1.75×10^{-9}	60.521	Tsang and Herron[36] [c]

[a] The values for A and E_a given here were evaluated from the rate constant data of ref 22a for the experiments performed with Ar diluent. [b] The rate expression recommended in ref 35, $k_1(T) = 1.15T^{-2.5} \exp(-65.001 \text{ kcal mol}^{-1}/RT)$ cm^3 molecule^{-1} s^{-1}, $T = 1500 - 3600$ K, was reevaluated by using least-squares analysis to give a linear fit over the temperature range $T = 1500 - 2500$ K. [c] The rate expression recommended in ref 36, $k_1(T) = 1.2 \times 10^{-6}T^{-0.73} \exp(-65.001 \text{ kcal mol}^{-1}/RT)$ cm^3 molecule^{-1} s^{-1}, T = 700 − 2500 K, was reevaluated by using least-squares analysis to give a linear fit over the temperature range $T = 1000 - 2500$ K. The expression tabulated here is for M = Ar (corrected for collision efficiency: $[Ar] = [N_2]/1.5$).

TABLE 2: High-Pressure Rate Constants for $N_2O + M \rightarrow N_2 + O\ (^3P) + M$

temperature (K)	pressure (Torr)	A_∞ (s^{-1})	E_a (kcal mol^{-1})	refs
1400−2500	(6.08×10^2)−(2.28×10^5)	1.26×10^{11}	59.5	Olschewski *et al.*[12]
1250−1800	(5.32×10^3)−(7.60×10^3)	9.3×10^{10} [a]	52.8	Verem'ev *et al.*[38]
1780−2300	(1.52×10^3)−(1.55×10^4)	1.7×10^{11}	57.6	Zuev *et al.*[39]
1103−1173	(1.14×10^3)−(7.98×10^3)	5.3×10^{10} [a]	56.02	Allen *et al.*[2]
1600−2000	(2.28×10^2)−(3.42×10^5)	1.3×10^{12}	62.61	Röhrig *et al.*[15]

[a] This value has been corrected for collision efficiency: $[Ar] = [N_2]/1.5$.

et al.,[12b] and Rohrig *et al.*,[15] along with those from two other investigations[38,39] and three review articles.[34−36] The recent study of Rohrig *et al.*[15] reports results that cover an exceptionally wide range in total pressure (argon buffer gas, about 0.3−450 atm) and, although there is considerable scatter in the data, the derived activation energy for the rate constant at the high-pressure limit implies that the singlet−triplet crossing occurs at about 63 kcal mol^{-1} above the singlet ground state. This value for E_a^∞, which is some 3.4 kcal mol^{-1} higher than that reported previously[12b,34−36] (59.6 kcal mol^{-1}) and adopted in theoretical calculations, would appear to support the consensus ARAS value for E_a^o of about 61 kcal mol^{-1}. However, Rohrig *et al.*[15] report an Arrhenius E_a^o value of 55.8 ± 1 kcal mol^{-1} for the temperature range 1688−3113 K, in good agreement with the values given in refs 34−36. Clearly, a precisely defined kinetic expression for the low-pressure rate constant is required to test future unimolecular calculations and for modeling of combustion systems.

A full description of N_2O thermal decomposition requires that reactions R2a and R2b be considered along with reaction R1, particularly at low temperatures:

$$O(^3P) + N_2O \rightarrow NO + NO \qquad \text{(R2a)}$$

$$O(^3P) + N_2O \rightarrow N_2 + O_2 \qquad \text{(R2b)}$$

At high concentrations of N_2O and where substantial decomposition takes place, the following additional reactions may also become significant:

$$O(^3P) + NO + Ar \rightarrow NO_2 + Ar \qquad \text{(R3)}$$

$$O(^3P) + NO_2 \rightarrow O_2 + NO \qquad \text{(R4)}$$

$$NO + N_2O \rightarrow NO_2 + N_2 \qquad \text{(R5)}$$

$$O(^3P) + O_2 + Ar \rightarrow O_3 + Ar \qquad \text{(R6)}$$

$$NO + O_3 \rightarrow NO_2 + O_2 \qquad \text{(R7)}$$

Few values for the rate constants of reactions R2a and R2b have been reported. The reaction is relatively slow, and until recently, both channels were thought to be of nearly equal importance, $k_{2a} = 1.1 \times 10^{-10} \exp(-13400/T)$ cm^3 molecule^{-1} s^{-1} (refs 35 and 36), $k_{2b} = 1.7 \times 10^{-10} \exp(-14100/T)$ cm^3 molecule^{-1} s^{-1} (refs 35 and 36), although the experimental evidence for this conclusion is sparse.[34−37] However, a recent study[40] has reported significantly different rate constant expressions for the two channels: $k_{2a} = (4.8 \pm 15\%) \times 10^{-11} \exp(-11650/T)$ cm^3 molecule^{-1} s^{-1} ($1680 \le T \le 2430$ K, 0.7−1.0 atm) and $k_{2b} = (2.3 \pm 25\%) \times 10^{-12} \exp(-5440/T)$ cm^3 molecule^{-1} s^{-1} ($1940 \le T \le 3340$ K, 0.9−2.0 atm). Values

of the bimolecular rate constant calculated from these equations at high temperatures, e.g., around 2000 K, agree with those from the recommended expressions,[34−36] but there are significant differences when the expressions are extrapolated to the important range of practical combustion systems, $1000 \leq T \leq 1500$ K. This observation was noted already by Allen *et al.*[2] in a recent paper on a variable pressure flow study of nitrous oxide. Specifically, they concluded (from detailed kinetic modeling calculations in their experimental temperature range $1103 \leq T \leq 1173$ K) that values of the overall rate constant for the O + N_2O reactions obtained by extrapolating the expression of Davidson *et al.*[40] were too large. The low activation energy for reaction R2b of 10.8 kcal mol^{-1} determined by Davidson *et al.*[40] is the primary reason for the large overall k_2 value at lower temperatures. These recent values also raise questions about the stoichiometric number[2,15] assumed in a previous study of N_2O dissociation.[12b]

In the present study, an O-atom spectrophotometer was calibrated. Bimolecular rate constant values for reaction R1 were determined over the temperature range $1195 \leq T \leq 2384$ K, taking into account absorption of resonance and nonresonance light by N_2O. These values were then combined with the individual data points from previous ARAS investigations to give a composite bimolecular rate constant expression ($1195 \leq T \leq 2494$ K). Kinetic modeling was employed to demonstrate that the present results are not consistent with recommended values for k_2 ($k_{2a} + k_{2b}$). A statistical approach was used to evaluate the data of seven runs to derive estimated upper limit values for k_2 over the temperature range $1200 \leq T \leq 1400$ K.

Experimental Section

The shock tube apparatus, its operation, and its subsequent modifications have been fully described elsewhere.[41−46] In the present study, the shock tube was operated in the thermal mode.[46] ARAS[41,47] was used to monitor changes in the concentration of O(^{3}P) atoms.

The temperature (T_5), density (ρ_5), and pressure (P_5) in the reflected shock regime were calculated using ideal shock theory from the measured values of the incident shock velocity, the test gas composition, the initial temperature, and the initial pressure.[41,48,49] Vibrational equilibrium was assumed to be complete. When necessary, boundary layer effects were corrected for by a procedure that made use of the adiabatic equation of state and of the experimental measurements of the pressure changes occurring in the sample after passage of the incident and reflected shock waves.[41] Uncertainties in determining Mach numbers ranged from 0.5 to 1% leading to corresponding uncertainties in T_5 and ρ_5 of 1−2%.

The resonance lamp was operated at a pressure of 10 Torr with a mixture of 0.0862% of O_2 in He and a microwave power level of about 100 W. An O-atom filter,[42−45] which consisted of a second microwave discharge in a flowing mixture of 9.54% O_2 in He that was maintained at 8 Torr, was located between the lamp and the shock tube window. A vacuum UV CaF_2 window, placed in the optical path between the filter and the shock tube window, allowed transmission of the O-atom resonance triplet lines, centered at 130.4 nm, but effectively blocked the lower lying resonance line emissions from H and N atoms. The photomultiplier housing was purged by a steady flow of N_2. When the voltage signal from the photomultiplier was measured with the filter discharge on and off, the fraction of incident resonance radiation was determined. If f is the fraction of resonance radiation, I_o is the total incident intensity (V_o volts) and I_t is the transmitted intensity at time t (V_t volts), then ABS_t, the absorbance at time t, is given by eq 1:

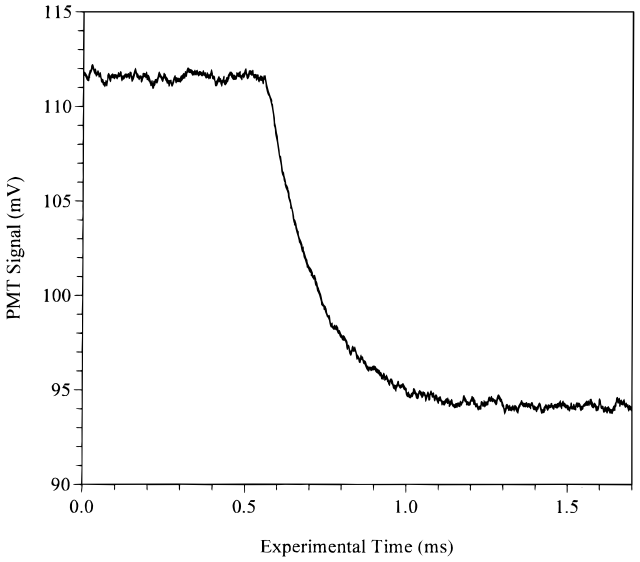

Figure 1. Typical transmission signal observed for the thermal decomposition of N_2O in the reflected shock regime: $P_1 = 15.64$ Torr, $M_s = 2.998$, $T_5 = 2163$ K, $\rho_5 = 3.32 \times 10^{18}$ molecules cm^{-3}, and $X_{N_2O} = 2.727 \times 10^{-6}$.

$$ABS_t = \ln[I_o f/(I_o f - (I_o - I_t))] = -\ln(1 - (V_o - V_t)/V_o f) \quad (1)$$

It is assumed that the Beer−Lambert law ($ABS = \alpha lC$) holds, where α is the O-atom absorption coefficient (cm^2 molecule^{-1}), l is the path length (the diameter of the shock tube, 6.02 cm), and C is the O-atom concentration (molecules cm^{-3}).

The base line level $I_o = V_o$ is usually taken as the signal level in the reflected regime immediately following the passage of the shock front past the observation window. At very high temperatures, where it can be obscured by the fast formation of atoms, the base line is determined from corresponding absorbance values associated with compression ratios measured at lower temperatures with appropriate concentrations of reactant mixtures. Where the rate constants were derived from the initial linear slope of the O-atom absorbance vs time, the base line could be easily determined with sufficient accuracy by extrapolation.

O-atom Calibration. The O-atom spectrophotometer was calibrated by completely dissociating N_2O at known mole fractions ($1.040 \times 10^{-6} \leq X_{N_2O} \leq 9.740 \times 10^{-6}$) in argon over the temperature range $1932 \leq T \leq 2384$ K. A typical transmittance−time profile from a calibration run is shown in Figure 1, the initial voltage signal rapidly decreasing with time after the passage of the reflected shock, to reach a constant level, corresponding to the final concentration of O-atoms when N_2O has fully dissociated. Experimental conditions are chosen so that secondary reactions are negligible, and therefore the final concentration of O-atoms $[O]_\infty$ is equal to the initial concentration of N_2O. A calibration plot can then be constructed that shows the relationship between absorbance and O-atom concentration.

Results from a total of 71 calibration runs are listed in Table 3 and plotted in Figure 2. The Beer−Lambert law holds up to absorbance values of approximately 0.67 (see Figure 2, inset), but at higher concentrations increasing curvature is observed. Over the total absorbance range, 0−1.1, the data are fitted by the polynomial of degree 2:

$$[O] = 8.127 \times 10^8 + (2.457 \times 10^{13})(ABS) + (6.123 \times 10^{12})(ABS)^2 \text{ atoms cm}^{-3} \quad (2)$$

TABLE 3: Calibration Data for the O-Atom Photometer[a]

P_1/(Torr)	M_s[b]	ρ_5[c]	T_5/K[d]	ABS_∞	ρ_5 (N_2O)[e]	P_1/(Torr)	M_s[b]	ρ_5[c]	T_5/K[d]	ABS_∞	ρ_5 (N_2O)[e]
					$X_{N_2O} = 1.040 \times 10^{-6}$						
15.11	2.947	3.173	2092	0.13	3.300	15.06	2.996	3.200	2159	0.13	3.328
15.11	2.959	3.181	2110	0.13	3.308						
					$X_{N_2O} = 1.058 \times 10^{-6}$						
15.07	2.971	3.200	2114	0.13	3.386	15.08	2.925	3.158	2056	0.13	3.341
15.07	2.936	3.160	2075	0.14	3.343	15.06	2.983	3.202	2132	0.14	3.388
15.00	2.887	3.108	2008	0.14	3.288	14.85	3.016	3.189	2173	0.13	3.374
14.89	2.963	3.151	2106	0.14	3.334	15.06	2.957	3.185	2095	0.14	3.370
					$X_{N_2O} = 1.655 \times 10^{-6}$						
15.53	2.929	3.245	2069	0.21	5.370	15.63	2.824	3.172	1932	0.20	5.250
					$X_{N_2O} = 2.014 \times 10^{-6}$						
15.00	2.892	3.112	2014	0.27	6.268	14.98	3.004	3.204	2159	0.27	6.453
15.08	2.884	3.126	2000	0.26	6.296	15.03	3.019	3.228	2179	0.27	6.501
15.06	2.921	3.153	2050	0.26	6.350	15.06	2.948	3.173	2086	0.26	6.390
15.07	2.937	3.165	2072	0.25	6.374						
					$X_{N_2O} = 2.322 \times 10^{-6}$						
15.06	3.025	3.224	2198	0.26	7.486	15.03	2.860	3.083	1976	0.26	7.159
15.00	3.095	3.261	2296	0.27	7.572	15.02	3.021	3.212	2192	0.27	7.458
					$X_{N_2O} = 2.404 \times 10^{-6}$						
15.06	2.897	3.125	2024	0.29	7.513	15.02	3.157	3.312	2383	0.28	8.001
14.98	3.030	3.209	2204	0.30	7.714	15.04	3.165	3.328	2391	0.28	7.963
15.05	2.864	3.087	1984	0.29	7.421	15.00	3.053	3.234	2235	0.29	7.774
10.30	3.143	2.266	2361	0.22	5.447	15.08	3.082	3.272	2276	0.30	7.866
					$X_{N_2O} = 2.727 \times 10^{-6}$						
15.74	3.118	3.476	2305	0.32	9.479	14.91	2.973	3.158	2122	0.32	8.612
15.65	2.903	3.254	2029	0.32	8.874	15.64	2.998	3.324	2163	0.32	9.065
					$X_{N_2O} = 3.150 \times 10^{-6}$						
14.94	2.967	3.151	2120	0.37	9.926	15.14	2.921	3.157	2059	0.37	9.945
15.15	2.924	3.160	2063	0.36	9.954						
					$X_{N_2O} = 3.266 \times 10^{-6}$						
15.05	3.011	3.212	2178	0.39	10.490	14.99	3.027	3.200	2208	0.37	10.451
15.09	3.028	3.225	2206	0.36	10.533	15.02	2.873	3.092	1995	0.39	10.098
					$X_{N_2O} = 4.120 \times 10^{-6}$						
15.02	3.107	3.278	2311	0.48	13.505	15.23	2.947	3.198	2091	0.50	13.176
15.03	2.965	3.171	2116	0.49	13.065	15.05	3.108	3.288	2311	0.47	13.547
					$X_{N_2O} = 5.191 \times 10^{-6}$						
15.04	3.035	3.270	2182	0.59	16.974	15.06	2.879	3.107	2001	0.60	16.128
15.02	3.032	3.239	2194	0.60	16.814	15.03	2.983	3.188	2139	0.57	16.549
15.13	3.033	3.239	2213	0.58	16.184						
					$X_{N_2O} = 5.807 \times 10^{-6}$						
14.98	3.034	3.220	2205	0.66	18.699	14.92	3.056	3.221	2237	0.64	18.704
15.02	3.029	3.223	2200	0.67	18.716	15.07	2.843	3.079	1954	0.67	17.880
					$X_{N_2O} = 7.755 \times 10^{-6}$						
14.88	2.995	3.185	2142	0.86	24.700	15.02	2.914	3.153	2030	0.86	24.451
15.29	3.000	3.273	2150	0.84	25.382	15.41	3.106	3.384	2295	0.83	26.243
15.05	2.935	3.171	2063	0.86	24.591						
					$X_{N_2O} = 9.740 \times 10^{-6}$						
15.33	2.995	3.287	2137	1.00	32.015	15.03	3.047	3.259	2211	0.97	31.743
15.08	2.990	3.230	2131	1.00	31.460	15.17	2.891	3.155	2006	1.06	30.730
					X_{N_2O}[f] $= 3.956 \times 10^{-6}$						
15.85	2.957	3.366	2087	0.49	1.332	15.76	3.091	3.451	2270	0.51	1.365
15.87	3.086	3.477	2262	0.50	1.376	15.32	3.174	3.436	2376	0.50	1.359
15.80	2.945	3.381	2051	0.49	1.338	15.23	3.174	3.404	2384	0.50	1.347

[a] Unless otherwise stated, the N_2O sample was of 99.99% purity. [b] The uncertainty in measuring the Mach number is typically about ±0.7% at the one standard deviation level. [c] Units of density are 10^{18} molecules cm^{-3}. [d] The uncertainty in temperature is estimated to be no more than ±1.5%. [e] Units of density are 10^{12} molecules cm^{-3}. [f] The N_2O sample for these data was of 99.999% purity.

The mean deviation of the experimental data points from those predicted by this expression is ±3.2%.

In general, rate constants in this study were evaluated only from absorbance data obtained in the concentration range over which the Beer−Lambert law held. From the zero constrained plot, Figure 2 (inset), a value for αl of $(3.66 \pm 0.06) \times 10^{-14}$ cm^3 $atom^{-1}$ was determined, independent of temperature over the experimental range of $1932 \leq T \leq 2384$ K. This value of αl corresponds to an O-atom absorption coefficient of 6.08×10^{-15} cm^2 $atom^{-1}$ showing, as expected, that there is appreciable self-absorption and pressure broadening in the lamp. This absorption coefficient is assumed to be constant over the total experimental temperature range of $1195 \leq T \leq 2384$ K. There were no significant changes in the values of the O-atom concentrations when they were calculated by eq 2. Six of the calibration runs ($X_{N_2O} = 3.956 \times 10^{-6}$), listed in Table 3 and shown in Figure 2 as filled circles, were performed using a separate source of N_2O (M. G. Products, stated purity of

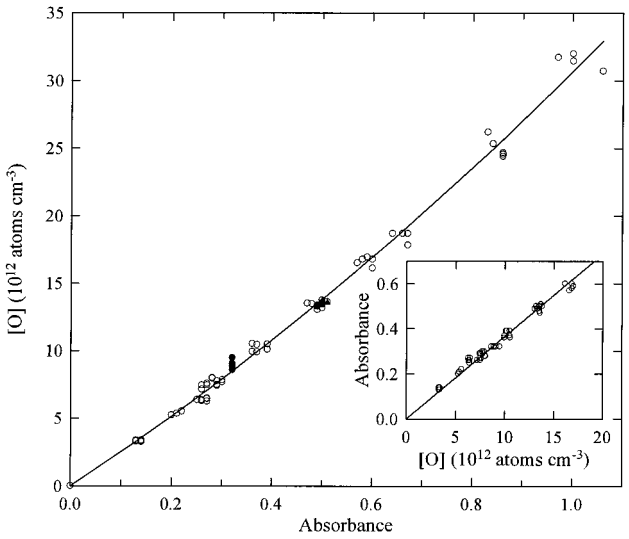

Figure 2. Calibration data. Solid line is fit of the polynomial of degree 2, $[O] = 8.127 \times 10^8 + (2.457 \times 10^{13})(ABS) + (6.123 \times 10^{12})(ABS)^2$ atoms cm^{-3}, to absorbance data from 0 to 1.1: open circle, data from purified 99.99% N_2O, filled circle, data from purified 99.999% N_2O. Inset: solid line is the linear least-squares fit of the Beer−Lambert expression, $ABS = \alpha l[O]$, where $\alpha l = 3.66 \times 10^{-14}$ cm^3 atom^{-1}, over the absorbance range $0-0.6 \equiv 0-1.7 \times 10^{13}$ atoms cm^{-3}.

99.999%). These points were in excellent agreement with the other calibration data. It was observed that the calibration of the lamp was reproducible over a long period of time provided that the lamp operating conditions were the same and that the lamp was tuned and conditioned after each shutdown period. In experiments where the light fraction at room temperature was deliberately changed by altering the lamp operating conditions, it was shown that, for the high-temperature runs, calibration and kinetic data were independent of the light fraction. From these observations, it can be inferred that the O-atom filter technique worked efficiently and that the measurements were not dependent of the output characteristics of the lamp. As part of the experimental procedure, the calibration was checked periodically by performing measurements at temperatures of about 2100 K, where N_2O completely dissociates during the observation time.

Molecular Absorption at High Concentrations of N_2O. Incident radiation from resonance H and O-atom lamps contains a significant fraction of nonresonance light that can range from 10 to 35% depending on lamp operating conditions. The resonance light fraction *f*, necessary for the calculation of absorbance and atom concentration, is usually determined at ambient temperature for the evacuated shock tube as has been previously described.[41] In general, the absorption coefficients of molecular components at resonance wavelengths are very much less than those of the H and O-atoms, ranging from $10^{-18}-10^{-20}$ cm^2 molecule^{-1}. These values are to be compared to absorption coefficients of $10^{-13}-10^{-14}$ cm^2 atom^{-1} for H atoms and $10^{-14}-10^{-15}$ cm^2 atom^{-1} for O-atoms observed with typical resonance lamps. Careful tuning of the microwave cavity, the lamp design itself, and appropriate choice of operating conditions enable bright, stable, and reproducible plasmas that emit 75−90% of incident resonance light to be formed. The use of a solar blind photomultiplier further minimizes the effect of absorption of nonresonance radiation by molecular components. Usually in the typical ARAS shock tube experiment, the small perturbations in the value of the light fraction, caused by light absorption by the molecular components of the mix, are not significant and thus the light fraction is little changed in the reflected regime. Moreover, these small perturbations have even a more minor effect on the accuracy of the rate constant determination, especially when compared to the typical errors that result from the uncertainties in determining the temperature, pressure, and density in the reflected regime.

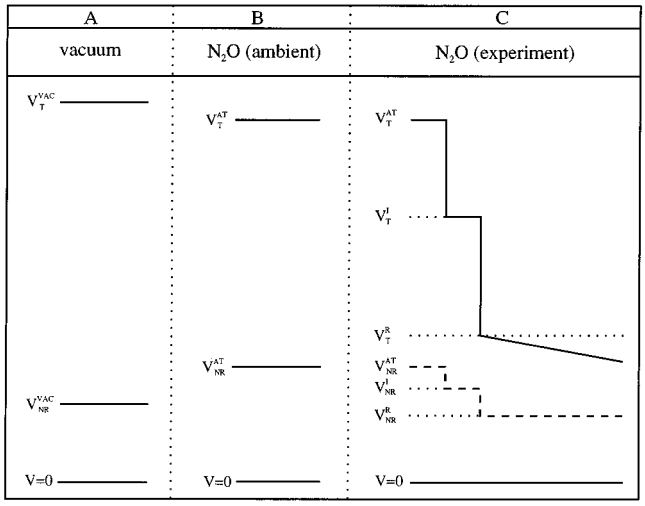

Figure 3. Schematic of transmission changes observed when a high concentration ($X_{N_2O} = 2.0 \times 10^{-2}$) N_2O mixture is shocked. (a) Solid lines are signal levels in evacuated shock tube: $V^{VAC}{}_T$, O-atom filter off and $V^{VAC}{}_{NR}$, O-atom filter on. (b) Corresponding signal levels in shock tube filled with N_2O mixture. Note high voltage on photomultiplier tube has been increased. (c) Signal levels observed when mixture is shocked: solid lines are observed signals and dashed lines are corresponding signal levels with filter on; they are not observed and must be calculated, see text. Superscripts: VAC, evacuated shock tube; AT, ambient temperature; I, incident regime; R, reflected regime. Subscripts: T, total signal, filter off and NR, nonresonance signal, filter on.

Nitrous oxide, however, is a relatively strong absorber of both the resonance and nonresonance wavelengths to which the typical solar blind photomultiplier is sensitive.[50] Neglect of this absorption, particularly at the higher concentrations required for the lower temperatures in this study, can lead to serious errors in the determination of absorbance values and, hence, of O-atom concentrations and rate constants. The simplest method to take this effect into account is to determine the light fraction in the reflected regime directly by carrying out the same experiment, with and without the filter on, in separate but identical shocks. Unfortunately, as is well-known, it is characteristic of the shock tube technique that identical shocks cannot be generated consistently; exact conditions of temperature and density in the reflected regime are notoriously difficult to duplicate on demand. Hence, the following experimental procedure was devised. A series of experiments with N_2O/Ar mixtures of appropriate compositions were carried out with the filter on, i.e., with only nonresonance light being transmitted through the shock tube. From the changes in transmittance and $[N_2O]$ resulting from successive incident and reflected shock compressions, a calibration curve was constructed for absorbance of nonresonance light by N_2O, ABS_{NR} vs $\Delta[N_2O]$, where $\Delta[N_2O]$ is the difference between N_2O concentration in the incident and reflected shock regime and that at ambient temperature prior to shock processing. This procedure is presented schematically in Figure 3, where $ABS^R{}_{NR} = \ln(V^{AT}{}_{NR}/V^R{}_{NR})$ and $ABS^I{}_{NR} = \ln(V^{AT}{}_{NR}/V^I{}_{NR})$. The symbols are defined as follows: (*superscripts*) AT, ambient temperature; *I*, incident regime; R, reflected regime; and VAC, shock tube under vacuum; and (*subscripts*) NR, nonresonance radiation and T, total (nonresonance + resonance radiation).

TABLE 4: Absorbance Data: Nonresonance Light (O-Atom Filter On)

V^{AT}_{NR}[a]	V^{I}_{NR}[b]	V^{R}_{NR}[c]	ABS^{I}_{NR}[d]	$\Delta[N_2O]$[e]	ABS^{R}_{NR}[f]	$\Delta[N_2O]$[g]
32.83	28.02	24.07	0.1584	1.864	0.3104	5.035
35.21	30.88	27.00	0.1312	1.511	0.2655	4.035
26.00	24.78	23.57	0.0480	0.3659	0.0980	0.9801
52.36	44.97	38.80	0.1521	1.825	0.2997	5.174
52.38	44.77	38.45	0.1570	1.641	0.3092	4.643
54.59	48.61	42.85	0.1160	1.079	0.2421	3.090
55.61	50.41	45.25	0.0982	0.8663	0.2062	2.447
56.76	50.68	44.93	0.1133	1.034	0.2337	2.763
57.19	51.29	45.64	0.1089	1.012	0.2256	2.724
58.12	53.37	48.24	0.08537	0.7159	0.1865	2.028
47.78	43.88	39.56	0.08517	0.7100	0.1889	2.010
45.91	42.81	39.10	0.06995	0.5673	0.1606	1.622
27.65	26.31	24.62	0.04968	0.3765	0.1161	1.015

[a] Initial voltage level at room temperature before shock compression; units are mV. [b] Voltage level after incident shock compression; units are mV. [c] Voltage level after reflected shock compression; units are mV. [d] Nonresonance absorbance after incident shock compression; $ABS^{I}_{NR} = \ln(V^{AT}_{NR}/V^{I}_{NR})$. [e] Change in N_2O concentration after incident shock compression; units are molecules $cm^{-3} \times 10^{15}$. [f] Nonresonance absorbance after reflected shock compression; $ABS^{R}_{NR} = \ln(V^{AT}_{NR}/V^{R}_{NR})$. [g] Change in N_2O concentration after reflected shock compression; units are molecules $cm^{-3} \times 10^{15}$.

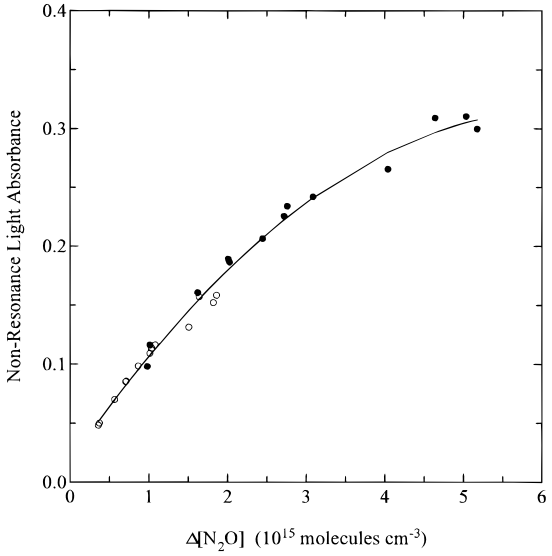

Figure 4. Calibration curve for determination of the nonresonant light absorbance by N_2O. Solid line is fit of the polynomial of degree 2, $ABS_{NR} = 1.744 \times 10^{-2} + (9.674 \times 10^{-17})(\Delta[N_2O]) - (7.857 \times 10^{-33})(\Delta[N_2O])^2$, to experimental data over $\Delta[N_2O]$ range of $(0.37-5.2) \times 10^{15}$ molecules cm^{-3} (Table 4); open circle, data from incident regime; filled circle, data from reflected regime.

The calibration data are listed in Table 4 and shown in Figure 4. This procedure was necessary only for the low end of the temperature range ($1195 \leq T \leq 1602$ K), where higher mole fractions of N_2O were required to obtain adequate O-atom absorbances. It was assumed that the absorption coefficient for N_2O for nonresonance light was constant. A polynomial fit to the data gave the following expression for ABS_{NR}, which is a function only of $\Delta[N_2O]$:

$$ABS_{NR} = 1.744 \times 10^{-2} + (9.674 \times 10^{-17})(\Delta[N_2O]) - (7.857 \times 10^{-33})(\Delta[N_2O])^2 \quad (3)$$

The mean deviation of the experimental points from this fit was ±4.0%. From this equation, ABS_{NR} could be calculated for any value of $\Delta[N_2O]$ in the reflected regime; hence from the Beer−Lambert law, $V^{R}_{NR} = V^{AT}_{NR} \exp(-ABS_{NR})$, the appropriate voltage level for nonresonance light V^{R}_{NR} in the reflected regime could be determined. The value of V^{AT}_{NR} for each experiment was calculated from the measured V^{AT}_{T}, the base line before the shock (see Figure 3), by making use of the light fraction f^{AT} previously determined for the particular mix at ambient temperature. Hence, from the experimentally determined V^{R}_{T} value, the correct light fraction for the reflected regime could be calculated. In summary, the light fraction for the evacuated shock tube $f^{VAC} = (V^{VAC}_{T} - V^{VAC}_{NR})/V^{VAC}_{T}$, was measured. The shock tube was then filled, and the light fraction, $f^{AT} = (V^{AT}_{T} - V^{AT}_{NR})/V^{AT}_{T}$, was measured at ambient temperature for the particular mix. The mixture was shocked and the correct value for the light fraction in the reflected regime, $f_{CORR} = (V^{R}_{T} - V^{R}_{NR})/V^{R}_{T}$, calculated by the above procedure. Absorbance values were then calculated in the usual manner from eq 1.

TABLE 5: Effect of Changing Light Fraction Value on Rate Constants

T (K)	X_{N_2O}	light fraction (uncorrected, f^{AT})	light fraction (corrected, f_{CORR})	percent change[a]
1500	2.403×10^{-4}	0.65	0.62	5.3
1378	2.403×10^{-4}	0.63	0.58	8.1
1409	4.176×10^{-4}	0.64	0.56	16.0
1425	1.000×10^{-3}	0.62	0.50	33.0
1322	2.000×10^{-3}	0.69	0.38	150.0

[a] Percentage change in rate constants (as presented in Table 7) that employed the correct light fraction.

Depending upon the mole fraction of N_2O and the temperature, the resonance light fraction decreased in going from vacuum to sample at ambient temperature to sample in the reflected regime. The effect of typical changes in the light fraction on the measured rate constant values for five examples are listed in Table 5. Use of the corrected light fraction f_{CORR} always leads to larger absorbance values, i.e., larger concentration of O-atoms, and thus to an increase in the value of the derived rate constant. This effect is most pronounced for results obtained at low temperatures where high concentrations of N_2O were generally employed.

Materials. The helium and argon were of stated purity of 99.9999% (M. G. Industries). The two nitrous oxide samples (99.99% and 99.999%, M. G. Industries) were further purified by the freeze−pump−thaw technique at 78 K. The 0.0862% O_2/He and 9.54% O_2/He mixtures (both were 99.999% purity O_2 and 99.9999% purity He, M. G. Industries) were used directly from cylinders without further purification.

Results and Discussion

The N_2O + M(Ar) Reaction. As discussed in the Introduction, the rate constant for reaction R1 has been demonstrated to be in the low-pressure limit for pressures ≤6 atm. Since the present experiments were performed at pressures below 1 atm, the data were computed as second-order rate constants.

Kinetic Analysis: First-Order Method. At high temperatures ($T > 1900$ K) the reaction goes to completion within the experimental observation time, and the low-pressure unimolecular rate, first order in [Ar] and $[N_2O]$, is then given by

$$-d[N_2O]_t/dt = d[O]_t/dt = k_1[Ar][N_2O]_t \quad (4)$$

Hence, k_1 can be determined from the slope of the first-order plot,

$$\ln([O]_\infty - [O]_t) = -k_{obs}t + \ln[O]_\infty \quad (5)$$

where $k_{obs} = k_1[Ar]$.

It already has been shown that for the present ARAS lamp, the Beer−Lambert law (ABS = αl[O]) holds up to absorbance values of about 0.7, and over this range, eq 5, on substitution, is transformed to

$$\ln(\mathrm{ABS}_\infty - \mathrm{ABS}_t) = -k_{\mathrm{obs}}t + \ln \mathrm{ABS}_\infty \qquad (6)$$

or, in the exponential form,

$$\mathrm{ABS}_t = \mathrm{ABS}_\infty (1 - \exp(-k_{\mathrm{obs}}t)) \qquad (7)$$

Figure 5 shows a typical absorbance−time plot, corresponding to the transmittance trace illustrated in Figure 1. The solid line through the data points is the fit to the first-order buildup equation (eq 7):

$$\mathrm{ABS}_t = 0.32(1 - \exp((-5925 \pm 26)t)) \qquad (8)$$

where $\mathrm{ABS}_\infty = 0.32$, $k_{\mathrm{obs}} = 5925 \pm 26$ s^{-1}, and [Ar] = 3.324×10^{18} molecules cm^{-3}; hence, $k_1 = 1.78 \times 10^{-15}$ cm^3 molecule^{-1} s^{-1}. Values of k_{obs} were obtained from linear least-squares fitting of eq 7 and are listed in Table 6 together with the corresponding values of k_1.

Kinetic Analysis: Initial Slope Method. At temperatures lower than about 1900 K, there was insufficient time to observe complete N_2O dissociation. On the other hand, given the time resolution and sensitivity of the apparatus, conditions could be readily chosen so that only a negligible fraction of N_2O was decomposed in the time frame of the experiment, and thus $[N_2O]_t \cong [N_2O]_o$ at all times. The rate constants could then be determined from the initial slopes of the absorbance−time profiles:

$$-\mathrm{d}[N_2O]_t/\mathrm{d}t = \mathrm{d}[O]_t/\mathrm{d}t = (\mathrm{dABS}_t/\mathrm{d}t)/\alpha l = k_1[N_2O]_o[\mathrm{Ar}] \qquad (9)$$

and

$$\mathrm{dABS}_t/\mathrm{d}t = k_1 \alpha l [\mathrm{Ar}][N_2O]_o \qquad (10)$$

Hence,

$$\mathrm{ABS}_{t2} - \mathrm{ABS}_{t1} = k_1 \alpha l [\mathrm{Ar}][N_2O]_o (t_2 - t_1) \qquad (11)$$

where t_1 and t_2 are the arbitrary observation times.

The linear graph of ABS_t vs time (typical examples are shown in Figure 6) will have a slope (ABS s^{-1}) $\equiv k_1[N_2O]_o[\mathrm{Ar}]\alpha l$; hence, k_1 can be calculated by dividing by the known concentrations of N_2O and Ar and the value of αl (3.66×10^{-14} cm^3 atom^{-1}), which is assumed to be independent of temperature. Slopes were determined by the linear least-squares method, and the calculated k_1 values are listed in Table 7.

Arrhenius Expressions. *This study.* An Arrhenius plot of the kinetic data (131 points) from this study, listed in Tables 6 and 7, are shown in Figure 7. Over the temperature range $1195 \le T \le 2384$ K, and with total densities ranging from (2.266×10^{18})−(5.393×10^{18}) molecules cm^{-3}, the data were well represented by the Arrhenius expression:

$$k_1(T) = (1.18 \pm 0.16) \times 10^{-9} \exp[(-57820 \pm 460 \text{ cal mol}^{-1})/RT] \text{ cm}^3 \text{ molecule}^{-1} \text{ s}^{-1} \qquad (12)$$

The uncertainties are given at the 1σ standard deviation level, and the mean deviation of experimental data from the expression is ±24%.

In those experiments performed at high temperatures ($1932 \le T \le 2384$ K), first-order kinetic behavior was always observed, and no evidence of complex kinetics was apparent. This was as expected from results of simulation studies. Experimental values of $k_1(T)$ were independent of changes in $[N_2O]$, which was varied by more than a factor of 5 ((3.3×10^{12})−(1.8×10^{13})). This is further evidence that the first-order decay of N_2O was free from the influence of secondary reactions.

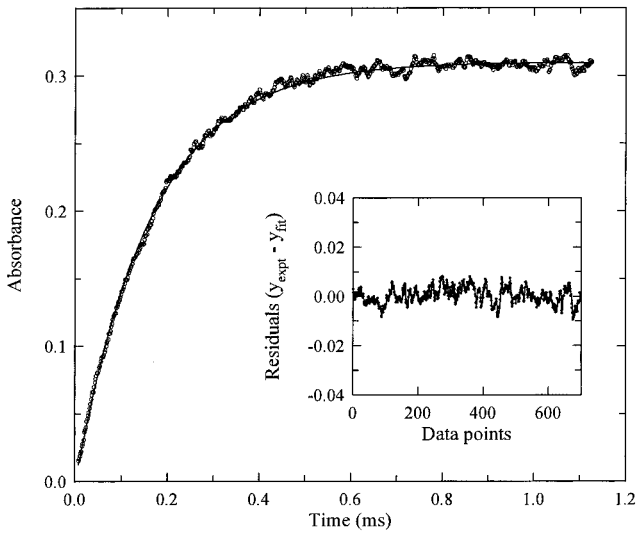

Figure 5. Plot of the absorbance buildup corresponding to the transmission signal of Figure 1: Open circle, experimental data points; solid line, fit of first-order equation, $\mathrm{ABS}_t = \mathrm{ABS}_\infty(1 - \exp(k_{\mathrm{obs}}t))$, where $k_{\mathrm{obs}} = 5925$ s^{-1}, $\mathrm{ABS}_\infty = 0.32$, $k_1 = k_{\mathrm{obs}}/[\mathrm{M}]$, $[\mathrm{M}] \equiv \rho_5 = 3.324 \times 10^{18}$ molecules cm^{-3}. Inset: plot of residuals. Here, time = 0 corresponds to the passage of the reflected shock by the observation window.

The total densities ρ_5(Ar) for the kinetic data reported in Tables 6 and 7 vary by a factor of 2.1 from (2.6×10^{18})−(5.4×10^{18}) molecules cm^{-3}. No systematic pressure dependence of the bimolecular rate constant k_1 was observed; thus, it was concluded that these experiments were performed in or near to the low-pressure limit. Other workers,[18−22] using the O-atom ARAS technique to investigate N_2O thermal decomposition, have reached similar conclusions, and in the study of Frank and Just,[18] experiments were extended to much higher total densities ((4.2×10^{18})−(36.1×10^{18}) molecules cm^{-3}) than those employed in the present study.

To check for impurity effects, experiments were also performed using a second source of N_2O that had a stated purity of 99.999%. The kinetic results obtained over the temperature range $1400 \le T \le 2384$ K and the calibration results were in excellent agreement with those from the experiments that employed 99.99% purity N_2O (see Figures 2 and 7).

Composite Data Set. The ARAS technique was employed previously by five groups to determine the unimolecular dissociation of N_2O in argon mixtures in the low-pressure limit. In Figure 8, the previous ARAS data appear to agree well with one another and with the present results for $k_1(T)$. Therefore, the results from this study were combined with the ARAS data sets of Roth and Just[18c] ($1498 \le T \le 2245$ K), Pamidimukkala et al.[19] ($1519 \le T \le 2408$ K), Frank and Just[20b] ($1389 \le T \le 2210$ K), Fujii et al.[21b] ($1602 \le T \le 2421$ K), and Michael and Lim[22b] ($1546 \le T \le 2494$ K) to obtain a composite ARAS data set of 278 data points, equal weight being given to each data point. Since tabulated data for $k_1(T)$ were not given in four of the five previous ARAS studies,[18c,20b,21b,22b] this is the first evaluation to make a detailed comparison among these studies. Linear-least squares analysis (Figure 8) results in the

TABLE 6: Rate Constant Data for the Reaction $N_2O + Ar \rightarrow N_2 + O(^3P) + Ar$: First-Order Analysis[a]

P_1/(Torr)	M_s[b]	ρ_5[c]	T_5/K[d]	k_{obs}[e]	k_1[f]	P_1/(Torr)	M_s[b]	ρ_5[c]	T_5/K[d]	k_{obs}[e]	k_1[f]
					$X_{N_2O} = 1.040\times10^{-6}$						
15.11	2.947	3.173	2092	4080	12.9	15.06	2.996	3.200	2159	5455	17.0
15.11	2.959	3.181	2110	4356	13.7						
					$X_{N_2O} = 1.058\times10^{-6}$						
15.07	2.971	3.200	2114	2934	9.17	15.08	2.925	3.158	2056	2144	6.79
15.07	2.936	3.160	2075	2853	9.03	15.06	2.983	3.202	2132	3299	10.3
15.00	2.887	3.108	2008	2395	7.71	14.85	3.016	3.189	2173	4455	13.9
14.89	2.963	3.151	2106	3230	10.2	15.06	2.957	3.185	2095	3453	8.38
					$X_{N_2O} = 1.655\times10^{-6}$						
15.53	2.929	3.245	2069	3223	9.93	15.63	2.824	3.172	1932	1402	4.42
					$X_{N_2O} = 2.014\times10^{-6}$						
15.00	2.892	3.112	2014	1852	5.95	14.98	3.004	3.204	2159	4869	15.2
15.08	2.884	3.126	2000	1706	5.46	15.03	3.019	3.228	2179	4164	12.9
15.06	2.921	3.153	2050	2312	7.33	15.06	2.948	3.173	2086	2784	8.77
15.07	2.937	3.165	2072	2469	7.80						
					$X_{N_2O} = 2.322\times10^{-6}$						
15.06	3.025	3.224	2198	6711	20.8	15.03	2.860	3.083	1976	1553	5.04
15.00	3.095	3.261	2296	14307	43.9	15.02	3.021	3.212	2192	6441	20.1
					$X_{N_2O} = 2.404\times10^{-6}$						
15.06	2.897	3.125	2024	1960	6.27	15.05	2.864	3.087	1984	2053	6.65
14.98	3.030	3.209	2204	7888	24.6						
					$X_{N_2O} = 2.727\times10^{-6}$						
15.74	3.118	3.476	2305	16708	48.1	14.91	2.973	3.158	2122	3957	12.5
15.65	2.903	3.254	2029	2064	6.34	15.64	2.998	3.324	2163	5925	17.8
					$X_{N_2O} = 3.150\times10^{-6}$						
14.94	2.967	3.151	2120	4274	13.6	15.14	2.921	3.157	2059	3713	11.8
15.15	2.924	3.160	2063	3457	10.9						
					$X_{N_2O} = 3.266\times10^{-6}$						
15.05	3.011	3.212	2178	5899	18.4	14.99	3.027	3.200	2208	8659	27.1
15.09	3.028	3.225	2206	8497	26.4	15.02	2.873	3.092	1995	1274	4.12
					$X_{N_2O} = 4.120\times10^{-6}$						
15.02	3.107	3.278	2311	14700	44.8	15.23	2.947	3.198	2091	3555	11.1
15.03	2.965	3.171	2116	4532	14.3	15.05	3.108	3.288	2311	13716	41.7
					$X_{N_2O} = 5.191\times10^{-6}$						
15.04	3.035	3.270	2182	7765	23.8	15.06	2.879	3.107	2001	1318	4.24
15.02	3.032	3.239	2194	7897	24.4	15.03	2.983	3.188	2139	5054	15.9
15.13	3.033	3.239	2213	7305	22.6						
					$X_{N_2O} = 5.807\times10^{-6}$						
14.98	3.034	3.220	2205	8405	26.1	14.92	3.056	3.221	2237	9651	30.0
15.02	3.029	3.223	2200	7973	24.7	15.07	2.843	3.079	1954	1662	5.4
					X_{N_2O}[g] $= 3.956\times10^{-6}$						
15.85	2.957	3.366	2087	2624	7.80	15.76	3.091	3.451	2270	12825	37.2
15.87	3.086	3.477	2262	9749	28.0	15.32	3.174	3.436	2376	18648	54.2
15.80	2.945	3.381	2051	2729	8.07	15.23	3.174	3.404	2384	18230	53.6
15.55	2.832	3.188	1928	767	2.41						

[a] Unless otherwise stated, the N_2O sample was of 99.99% purity. [b] The uncertainty in measuring the Mach number is typically about ±0.7% at the one standard deviation level. [c] Units of density are 10^{18} molecules cm^{-3}. [d] The uncertainty in temperature is estimated to be ±1.5% or less. [e] Units of k_{obs} are s^{-1}. [f] Units of k_1 are 10^{-16} cm^3 $molecule^{-1}$ s^{-1}. [g] The N_2O sample for these data was of 99.999% purity.

following Arrhenius expression for the temperature range $1195 \leq T \leq 2494$ K:

$$k_1(T) = (9.52 \pm 1.07)\times10^{-10}\exp[(-57570 \pm 390\ \text{cal mol}^{-1})/RT]\ \text{cm}^3\,\text{molecule}^{-1}\text{s}^{-1} \quad (13)$$

The mean deviation of the composite data set from eq 13 is ±26% (at the 1σ-level). The tightness of this fit may be contrasted to the systematic differences in the Arrhenius parameters between the individual ARAS data sets, which are readily discernable (values listed in Table 1). This work, therefore, further emphasizes that rate constants should be measured over as wide a temperature range as possible and that care should be taken to collect sufficient data points, especially in shock tube experiments.

It is evident from Figure 8 that, prior to the present study, few ARAS measurements of $k_1(T)$ have been reported at temperatures below 1500 K. Rate constant determinations for $k_1(T)$ were extended to just below 1200 K by making use of the correction procedure developed to take into account the significant molecular absorption of both resonance and non-resonance light by high concentrations of N_2O.

In Figure 9, these low-temperature measurements are seen to be in agreement with the (non-ARAS) rate constant data of Martinengo *et al.*[12a] (4 points over the temperature range $1320 \leq T \leq 1440$ K) and Glarborg *et al.*[1b] (4 points over the temperature range $1200 \leq T \leq 1348$ K). However, the non-ARAS data of Loirat *et al.*[23] (not shown) do not agree.

The six ARAS/shock tube studies that comprise the composite data set, employed total pressures from about 1 to 3 atm. The excellent agreement of these results over such a wide temperature range ($1195 \leq T \leq 2494$ K) is consistent with our previous conclusion (*viz.* Introduction) that reaction R1 is indeed in the low-pressure limit under the conditions of these studies. The

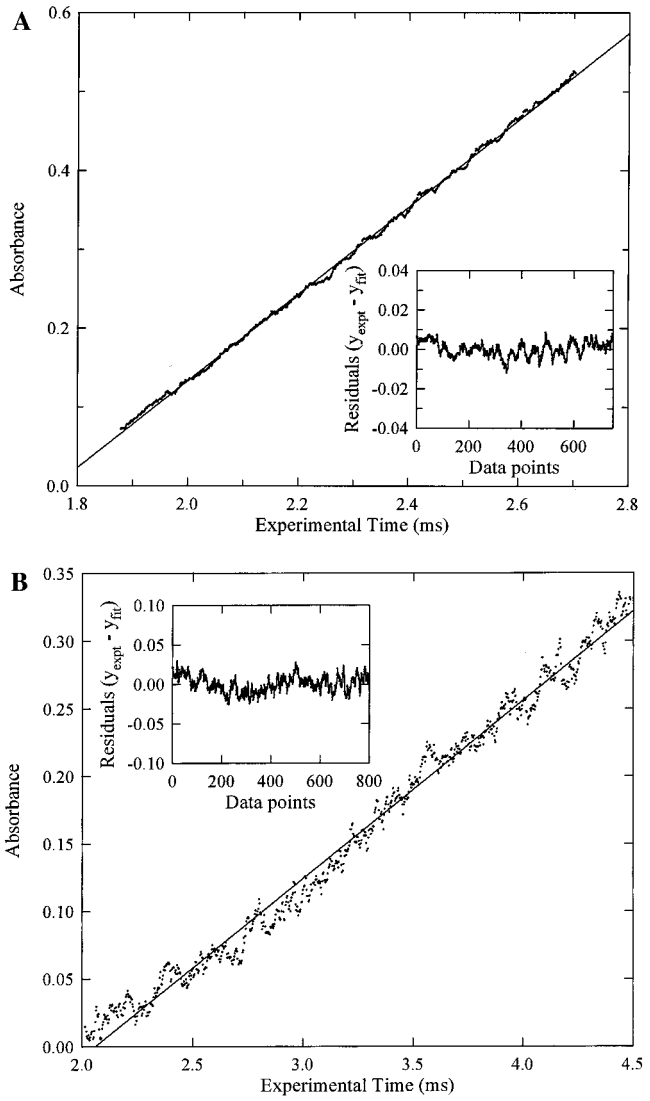

Figure 6. Examples of observed linear absorbance buildup plots at low temperatures. (a) $P_1 = 15.55$ Torr, $M_s = 2.509$, $T_5 = 1557$ K, $\rho_5 = 2.949 \times 10^{18}$ molecules cm^{-3}, $X_{N_2O} = 2.625 \times 10^{-4}$. Solid line: linear fit, gradient $= 551 \pm 0.57$ ABS s^{-1}, and $k_1 = 551/(3.66 \times 10^{-14} \times 2.949 \times 10^{18} \times 7.741 \times 10^{14}) = 6.59 \times 10^{-18}$ cm^3 molecule^{-1} s^{-1}. (b) $P_1 = 30.53$ Torr, $M_s = 2.253$, $T_5 = 1260$ K, $\rho_5 = 5.025 \times 10^{18}$ molecules cm^{-3}, $X_{N_2O} = 9.925 \times 10^{-4}$. Solid line: linear fit, gradient $= 132 \pm 0.52$ ABS s^{-1}, $k_1 = 132/(3.66 \times 10^{-14} \times 5.025 \times 10^{18} \times 4.987 \times 10^{15}) = 1.44 \times 10^{-19}$ cm^3 molecule^{-1} s^{-1}. Insets: plots of residuals.

individual data points of Rohrig *et al.*,[15] determined by monitoring IR emission from N_2O at 4.5 μm, are also in excellent agreement with the corresponding values calculated from eq 13. The deviations of their individual data points from those calculated ranged from −33% to +3% with a mean value of −14%. Moreover, these results are in agreement with the low-pressure data of Olschewski *et al.*[12b] (when account is taken of the uncertainty in the assumed stoichiometry[2,15]).

Over the temperature range $1195 \leq T \leq 2494$ K, there is no discernible curvature in the Arrhenius plot of the ARAS data, Figure 8, in agreement with the findings of Olschewski et al.,[12b] assuming that the stoichiometric number for the reaction is independent of temperature. An accurate temperature dependence of the low-pressure rate constant is difficult to predict without a detailed unimolecular calculation. However, if it is assumed that the rate of intersystem crossing of energized molecules is independent of energy (the Lindemann−Hinshelwood model), or that it has a very narrow energy distribution, then increasing the temperature from 1200 to 2500K would lead to a decrease in E_a^o of only a few kcal mol^{-1}. Also, even close to the high-pressure limit, where it is well established that the E_a^∞ is the difference between the average energy of the reacting levels from which intersystem crossing occurs and the average thermal energy of the molecule,[30] there is no evidence of curvature in the Arrhenius behavior.[12b,15] Finally, it may be possible that, at the highest temperatures, there is a small contribution from the more endothermic adiabatic dissociation process that leads to O(^{1}D). In the high-pressure limit, the unimolecular rate expression for this reaction should have an activation energy of about 84 kcal mol^{-1} ($\Delta H_0^o = 83.93$ kcal mol^{-1}, ref 9)as well as a preexponential factor that could increase by a factor of approximately 1000. The corresponding activation energy and preexponential factor for the low-pressure limit are difficult to estimate in the absence of a detailed unimolecular calculation. However, in the case of CH_4 dissociation, the activation energy in the low-pressure limit is lower than the endothermicity by about 18 kcal mol^{-1}.

O(^{3}P) + N_2O Reaction. The rate constants for the O + N_2O reactions R2a and R2b are difficult to measure experimentally because the overall reaction is very slow. Table 8 lists the rate expressions for reactions R2a and R2b recommended in three review articles[34−36] (including the recent recommendation of Tsang and Herron)[36] along with the expressions reported by Davidson *et al.*[40] (where rate constants were derived from measured O_2 and NO profiles).

The sensitivity of the O-atom ARAS technique lends itself to simplified kinetics and to a more direct method for determining the value for the overall rate constant, $k_2(k_{2a} + k_{2b})$. Analysis of the reaction sequence R1, R2a, and R2b leads to the following kinetic equations:

$$\begin{aligned} d[O]_t/dt &= k_1[N_2O][Ar] - k_2[N_2O][O]_t \\ &= k_1[N_2O][Ar](1 - (k_{2a} + k_{2b})[O]_t/k_1[Ar]) \end{aligned} \quad (14)$$

Under the present experimental conditions, it is readily shown that reactions R3−R7 can be neglected. On integration, the following expression for the buildup of the O-atom concentration is obtained:

$$[O]_t = k_1[Ar]/k_2(1 - \exp(-k_2[N_2O]t)) \quad (15)$$

where $k_2 = k_{2a} + k_{2b}$.

Kinetic modeling showed that deviation from initial linearity should be clearly observable over the temperature range $1200 \leq T \leq 1400$ K when recommended rate constants were employed. It was also shown that a high [N_2O] was required in order to obtain a sufficiently rapid buildup of [O] to enable curvature to be observed in the available experimental time frame (see eqs 14 and 15). Figure 10 shows the data from an experimental run at 1395K together with the results of two simulations (using the CHEMKIN[51] routine) that used the recommended values of k_2 from Tsang and Herron[36] and from Davidson *et al.*[40] Clearly the experimental data do not show the curvature that is evident in the simulations. All the experimental data in this investigation display similar behavior, and thus the present results do not support the use of k_2 values as large as those employed in the simulations. This suggests that k_2 must be even smaller than the recommended value of Tsang and Herron[36] and those of refs 34 and 35 (Table 8), since all three give very similar k_2 values over the temperature range of interest. Even though there is no evidence of strong curvature (as in the Figure 10 simulations) in any of the experimental initial-rate-data runs, upper limit values for k_2 can be estimated using the statistical approach described below.

TABLE 7: Rate Constant Data for the Reaction $N_2O + M \rightarrow N_2 + O(^3P) + M$: Initial Rate Analysis[a]

P_1[b]	M_s[c]	ρ_5[d]	T_5/(K[e])	rate[f]	k_1[g]	P_1[b]	M_s[c]	ρ_5[d]	T_5/(K[e])	rate[f]	k_1[g]
					$X_{N_2O} = 1.04 \times 10^{-6}$						
15.11	2.947	3.173	2092	431	112	15.11	2.959	3.181	2110	410	106
15.49	2.804	3.126	1906	87.6	23.6						
					$X_{N_2O} = 1.655 \times 10^{-6}$						
15.44	2.750	3.067	1838	125.5	22.0						
					$X_{N_2O} = 2.404 \times 10^{-6}$						
15.07	2.748	2.989	1837	154	19.5						
					$X_{N_2O} = 3.15 \times 10^{-6}$						
15.32	2.671	2.959	1744	40.6	4.02	14.81	2.776	2.959	1873	207	20.5
					$X_{N_2O} = 4.120 \times 10^{-6}$						
15.23	2.947	3.198	2091	1404	91.0	14.73	2.466	2.643	1503	4.60	0.437
15.03	2.965	3.171	2116	1671	110	14.97	2.630	2.858	1692	38.4	3.11
15.32	2.798	3.091	1896	426	29.5	17.09	2.519	3.132	1562	21.9	1.48
15.88	2.750	3.157	1836	193	12.8	16.62	2.584	3.120	1638	38.4	2.62
15.57	2.585	2.925	1639	48.8	3.77						
					$X_{N_2O} = 5.807 \times 10^{-6}$						
15.09	2.834	3.073	1944	897	44.8	15.14	2.641	2.904	1703	103	5.74
15.79	2.916	3.293	2048	1863	80.9	15.80	2.681	3.068	1754	116	5.79
15.39	2.946	3.233	2089	3075	138	14.97	2.736	2.962	1819	320	17.2
15.07	2.843	3.079	1954	987	48.9	14.96	2.722	2.948	1801	249	13.5
15.09	2.543	2.792	1589	24.5	1.48	15.14	2.626	2.902	1696	60.3	2.44
15.06	2.621	2.868	1680	33.0	1.89						
					$X_{N_2O} = 9.760 \times 10^{-6}$						
15.05	2.494	2.827	1549	30.5	1.07	15.26	2.536	2.835	1570	34.8	1.21
					$X_{N_2O} = 2.403 \times 10^{-4}$						
30.58	2.317	5.107	1335	51.1	0.0223	30.23	2.352	5.116	1378	92.0	0.0399
30.12	2.481	5.327	1519	1330	0.533	16.10	2.464	2.888	1500	661	0.902
					$X_{N_2O} = 2.548 \times 10^{-4}$						
32.73	2.265	5.318	1297	66.1	0.0251	27.17	2.347	4.681	1358	44.9	0.0220
25.53	2.402	4.433	1439	231	0.126	27.65	2.339	4.759	1346	53.0	0.0251
					$X_{N_2O} = 4.176 \times 10^{-4}$						
25.34	2.562	4.748	1602	3326	0.965	15.03	2.435	2.756	1484	732	0.631
25.53	2.344	4.371	1362	123	0.0421	15.08	2.375	2.725	1421	302	0.266
25.50	2.374	4.426	1393	198	0.0661	14.95	2.391	2.711	1441	393	0.350
25.45	2.389	4.449	1409	398	0.131	29.89	2.339	5.110	1355	150	0.0376
25.39	2.490	4.630	1519	1865	0.569	32.31	2.289	5.393	1294	104	0.0234
14.91	2.423	2.742	1470	468	0.407						
					$X_{N_2O} = 9.925 \times 10^{-4}$						
28.88	2.342	4.994	1344	212	0.0234	30.53	2.253	5.025	1260	132	0.0150
25.30	2.275	4.216	1282	92.8	0.0204						
					$X_{N_2O} = 1.010 \times 10^{-3}$						
15.05	2.381	2.729	1425	594	0.216	15.09	2.286	2.633	1333	126	0.0492
15.36	2.335	2.734	1381	413	0.149	24.08	2.277	3.997	1285	102	0.0173
					$X_{N_2O} = 1.482 \times 10^{-3}$						
20.97	2.226	3.437	1227	42.1	0.00657	19.78	2.154	3.284	1195	27.3	0.00467
19.42	2.215	3.314	1254	74.9	0.0148						
					$X_{N_2O} = 2.000 \times 10^{-3}$						
17.34	2.310	3.085	1344	237	0.0341	17.82	2.357	3.217	1395	336	0.0444
19.13	2.227	3.285	1265	168	0.0212	19.58	2.289	3.457	1322	189	0.0216
22.81	2.201	3.790	1232	124	0.0118						
					$X_{N_2O} = 2.014 \times 10^{-3}$						
15.48	2.270	2.705	1307	247	0.0458	15.71	2.278	2.736	1324	262	0.0475
					X_{N_2O}[h] $= 2.625 \times 10^{-4}$						
15.55	2.509	2.949	1557	551	0.659	15.46	2.399	2.800	1452	190	0.252
15.53	2.431	2.863	1479	160	0.203	15.04	2.390	2.724	1442	155	0.217
15.53	2.348	2.768	1400	49.9	0.0678	15.37	2.382	2.783	1429	93.6	0.126
15.48	2.464	2.871	1521	377	0.476						
					X_{N_2O}[h] $= 3.956 \times 10^{-6}$						
15.64	2.750	3.131	1823	156	11.0						

[a] Unless otherwise stated, the N_2O sample was of 99.99% purity. [b] Units are in Torr. [c] The uncertainty in measuring the Mach number is typically about ±0.7% at the one standard deviation level. [d] Units of density are 10^{18} molecules cm^{-3}. [e] The uncertainty in temperature is estimated to be no more than ±1.5%. [f] Units of rate are ABS s^{-1}. [g] Units of k_1 are cm^3 $molecule^{-1}$ $s^{-1} \times 10^{-17}$; k_1 = rate/(αl[N_2O][Ar]). [h] The N_2O sample for these data was of 99.999% purity.

Criteria. It was evident from the modeling studies that the O-atom buildup is most sensitive to the influence of reaction R2 (R2a + R2b) at low temperatures and for large mole fractions of N_2O. The following criteria were chosen for selecting data to analyze so that a consistent statistical approach could be employed in determining an upper limit for k_2: (i)

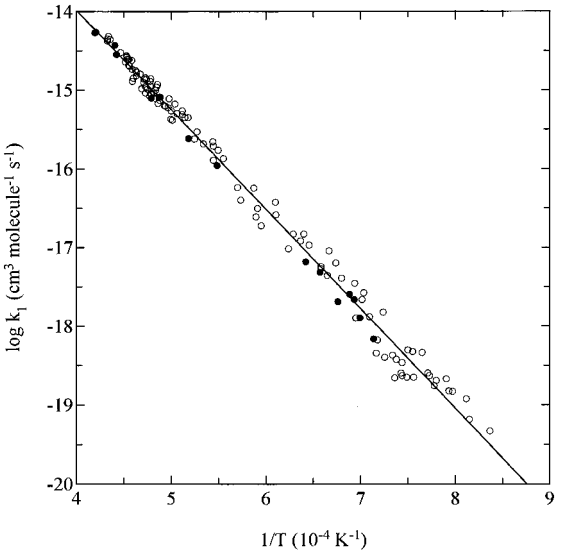

Figure 7. Arrhenius plot of the 131 data points (listed in Tables 5 and 6) for the reaction $N_2O + Ar \rightarrow N_2 + O(^3P) + Ar$ over the temperature range $1195 \leq T \leq 2384$ K. Solid line: linear least-squares fit, where $k_1(T) = (1.18 \pm 0.16) \times 10^{-9} \exp[(-57820 \pm 460 \text{ cal mol}^{-1})/RT]$ cm^3 molecule^{-1} s^{-1}. Open circle: 99.99% N_2O and filled circle: 99.999% N_2O.

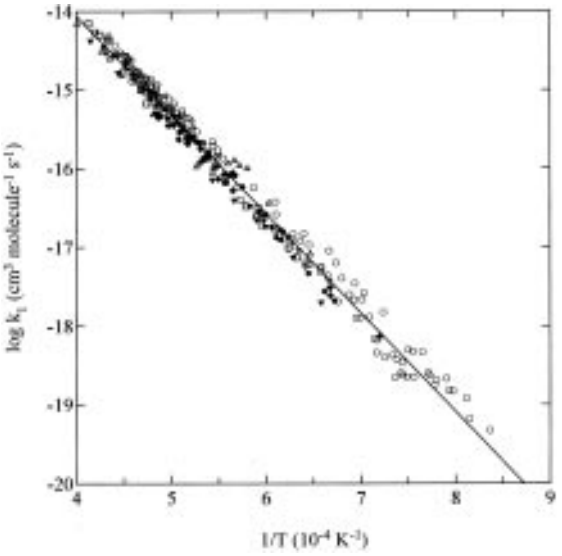

Figure 8. Arrhenius plot of the composite O-atom ARAS data set (278 points) for the low pressure rate constant, M = Ar: —, is the linear least squares fit, where $k_1(T) = (9.52 \pm 1.07) \times 10^{-10} \exp[(-57570 \pm 390 \text{ cal mol}^{-1})/RT]$ cm^3 molecule^{-1} s^{-1}; ○, this study ($1195 \leq T \leq 2384$ K); ▼, Pamidimukkala *et al.* ($1519 \leq T \leq 2408$ K); △, Michael and Lim ($1546 \leq T \leq 2494$ K); □, Fujii *et al.* ($1602 \leq T \leq 2421$ K); ♦, Frank and Just ($1389 \leq T \leq 2210$ K) ; ▽, Roth and Just ($1498 \leq T \leq 2245$ K).

low temperatures, to maximize the influence of reaction R2 *vis-a-vis* reaction R1; (ii) observation times (which depend on shock quality and lamp stability) greater than about 2ms, in order to increase the possibility of detecting the effect of k_2; and (iii) high [N_2O], with X_{N_2O} greater than about 1×10^{-3}, to allow sufficient buildup of the [O] at low temperatures. These criteria limited evaluation to seven runs over the approximate temperature range $1200 \leq T \leq 1400$ K.

Method of Analysis and Estimates of k_2. For each of the seven runs that met the criteria discussed above, values of k_2 were derived using the following procedure. First, k_1 and the standard deviation (σ) were determined by using a linear least-squares fit to the data in each of the experimental runs. This value of k_1 was increased by 2σ for the estimation of k_2 (the rationale

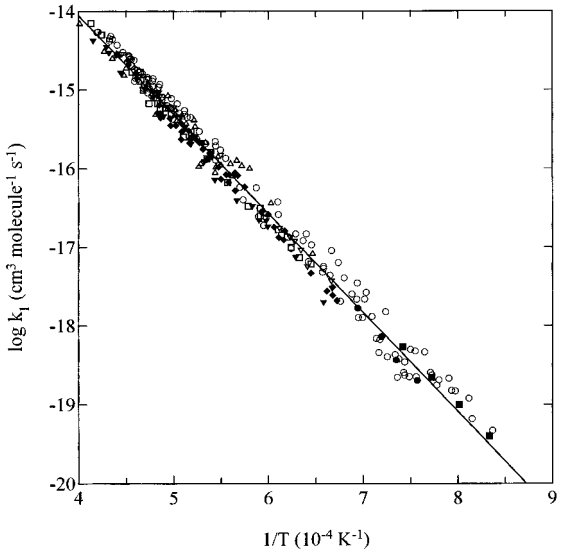

Figure 9. Arrhenius plot of all data (286 points): —, is the linear least-squares fit, where $k_1(T) = (9.45 \pm 1.00) \times 10^{-10} \exp[(-57540 \pm 370 \text{ cal mol}^{-1})/RT]$ cm^3 molecule^{-1} s^{-1}; ○, this study ($1195-2384$ K); ▼, Pamidimukkala *et al.* ($1519 \leq T \leq 2408$ K); △, Michael and Lim ($1546 \leq T \leq 2494$ K); □, Fujii *et al.* ($1602 \leq T \leq 2421$ K); ♦, Frank and Just ($1389 \leq T \leq 2210$ K); ▽, Roth and Just ($1498 \leq T$ Pound 2245 K); ■, Glarborg *et al.* ($1200 \leq T \leq 1348$ K); ●, Martinengo *et al.* ($1320 \leq T \leq 1440$ K).

TABLE 8: Rate Expressions for the $O(^3P) + N_2O$ Reaction

temperature (K)	rate expression (cm^3 molecule^{-1} s^{-1})	refs
1200−2000	$k_{2a} = 1.7 \times 10^{-10} \exp(-14100/T)$	Baulch *et al.*[34]
	$k_{2b} = 1.7 \times 10^{-10} \exp(-14100/T)$	
1200−4100	$k_{2a} = 1.1 \times 10^{-10} \exp(-13400/T)$	Hanson and Salimian[35]
	$k_{2b} = 1.7 \times 10^{-10} \exp(-14100/T)$	
1200−4100	$k_{2a} = 1.1 \times 10^{-10} \exp(-13400/T)$	Tsang and Herron[36]
	$k_{2b} = 1.7 \times 10^{-10} \exp(-14100/T)$	
1680−2430	$k_{2a} = 4.8 \times 10^{-11} \exp(-11650/T)$	Davidson *et al.*[40]
1940−3340	$k_{2b} = 2.3 \times 10^{-12} \exp(-5440/T)$	

for selecting 2σ is discussed below). The value of k_2 was then determined by using a nonlinear least-squares routine (Levenberg−Marquardt method[52]) to fit eq 15 to the data in each of the experimental runs. These k_2 values, corresponding to the upper limit in our evaluation, are listed in Table 9. These results clearly show that, over the narrow temperature range $1200 \leq T \leq 1400$ K, the estimated rate constant values for k_2 (the sum of k_{2a} and k_{2b}) are consistently lower than those calculated from the recommended expression of Tsang and Herron.[36] Values of k_2 ranged between about 4 and 32 times lower than the recommended ones. Even though there is large uncertainty (see further discussion below) in the k_2 values derived here, we believe these results show that, over the temperature range of the measurements, k_2 is about an order of magnitude smaller than that calculated from the expressions of Tsang and Herron.[36]

The uncertainties in the upper limit values for k_2 that were derived here are directly related to the perturbation of k_1 by $+2\sigma$. The 2σ level was selected because it always lead to observable curvature in the nonlinear fit to the absorbance data. At the 1σ level, curvature was just discernable and, at the 3σ level, the extent of curvature was very severe. These variations in the perturbation lead to about 0.5 times and 1.5 times the derived k_2 values, or an uncertainty of about 50% for the individual determinations. However, the scatter in the k_2 values is obviously greater than the estimated uncertainty level. We believe the large scatter is due to systematic error caused by modulation in the output of the resonance lamp. This "ripple" may result in data with random scatter or with slightly concave

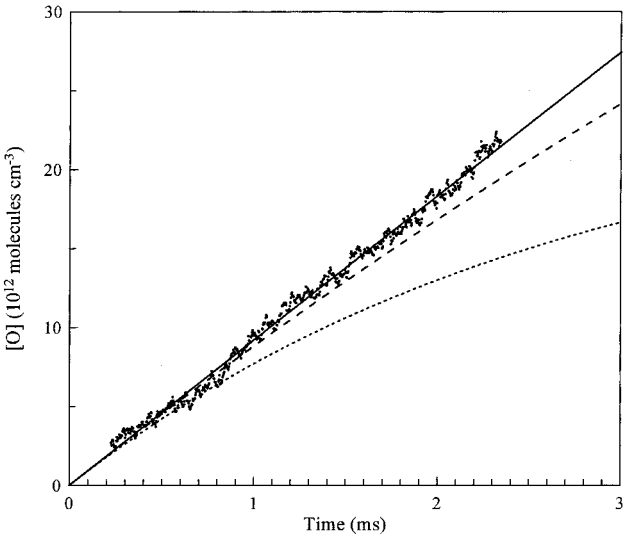

Figure 10. Influence of the O + N_2O reaction: comparison of experimentally observed buildup of O-atom concentrations with those predicted by appropriate kinetic modeling at $T = 1395$ K. Also, $P_1 = 17.82$ Torr, $M_s = 2.357$, $\rho_5 = 3.217 \times 10^{18}$ molecules cm^{-3}, $X_{N_2O} = 2.00 \times 10^{-3}$. Solid line is the linear least-squares fit, where $k_1 = 4.44 \times 10^{-19}$ cm^3 molecule^{-1} s^{-1}. For the dashed line, $k_1 = 4.44 \times 10^{-19}$ cm^3 molecule^{-1} s^{-1} and $k_2 = 1.43 \times 10^{-14}$ cm^3 molecule^{-1} s^{-1} (Tsang and Herron[36]). For the dotted line, $k_1 = 4.44 \times 10^{-19}$ cm^3 molecule^{-1} s^{-1} and $k_2 = 5.79 \times 10^{-14}$ cm^3 molecule^{-1} s^{-1}(Davidson *et al.*[40]).

TABLE 9: Rate Constant Data for the Reaction O(^{3}P) + N_2O

T (K)	X_{N_2O}	Δt (ms)	k_1[a]	σ[b]	k_2[c]	k_2(Tsang and Herron)/k_2[d]
1254	1.482×10^{-3}	3.192	1.48	6.43	5.4	8.8
1260	9.925×10^{-4}	2.704	1.50	5.80	1.6	31.7
1265	2.000×10^{-3}	2.584	2.12	13.16	9.6	5.4
1322	2.000×10^{-3}	2.252	2.16	10.20	13.1	6.3
1344	2.000×10^{-3}	2.815	3.41	12.10	3.2	31.0
1344	9.925×10^{-4}	1.896	2.34	8.69	23.5	4.2
1395	2.000×10^{-3}	2.345	4.44	13.36	8.5	16.8

[a] Units of k_1 are cm^3 molecule^{-1} s^{-1} $\times 10^{-19}$. [b] The standard deviation in k_1 from the linear fit of the [O] versus time data. Units are cm^3 molecule^{-1} s^{-1} $\times 10^{-22}$. [c] Units of k_2 are cm^3 molecule^{-1} s^{-1} $\times 10^{-16}$; the uncertainty in each determination is about 50%. [d] Ratio of the rate constant derived from the expression of Tsang and Herron[36] to the rate constant estimated in the present study.

or slightly convex curving O-atom buildup plots. For data with concave curvature, the derived values for k_2 were always too low (e.g., the values at 1260 and 1344 K/#1) and (conversely) for data with convex curvature, the derived values for k_2 were always too high (e.g., the values at 1322 and 1344 K/#2). The magnitude of this effect depends upon the O-atom buildup plots. In some cases, this effect was less than or about the same as the uncertainty in the individual determinations (e.g., the values at 1254, 1265, and 1395 K). In other cases, the effect was somewhat larger, say, about the same or as much as double the uncertainty in the individual determinations. Therefore, the values listed in Table 9 represent relatively crude estimates for the upper limit of k_2. At the most, however, we believe these values are not in error by more than about a factor of 3; and we therefore conclude that k_2 is much smaller than the value recommended by Tsang and Herron.[36] There is an even more serious difference between the upper limit value for k_2, derived here, and the value for k_2 computed from the expressions reported by Davidson *et al.*[40] The identification of this difference may not be important, however, because in the work reported by Rohrig *et al.*,[15] these authors not only question their ref 40 result but prefer the value recommended in the evaluation by Hanson and Salimian.[35]

Conclusions

Shock tube experiments were performed, with sensitive ARAS detection of oxygen atoms, to measure the rate constant for N_2O thermal dissociation at the low-pressure limit over the temperature range $1195 \leq T \leq 2384$ K. A procedure to correct for molecular absorption of resonance and nonresonance light by N_2O allowed rate constant measurements to be extended by almost 200° to just below 1200 K, which is significant in terms of $1/T$. Also, by extending measurements down to 1200 K, this work provides ARAS data for reaction R1 that, for the first time, overlap with previous studies that employed nonshock tube techniques. The present determinations at low temperatures demonstrate agreement with those reported by Martinengo et al.[12a] and Glarborg et al.[1b] but not with the data of Loirat et al.[23]

The ARAS rate data from five independent studies in five laboratories were combined with the present data for reaction R1 and represented by the Arrhenius expression,

$$k_1(T) = (9.52 \pm 1.07) \times 10^{-10} \exp[(-57570 \pm 390 \text{ cal mol}^{-1})/RT] \text{ cm}^3 \text{ molecule}^{-1} \text{s}^{-1} \quad (13)$$

over the temperature range $1195 \leq T \leq 2494$ K, where uncertainties are given at the 1σ level. The mean deviation of the composite data set from the Arrhenius expression (eq 13) is ±26% at the 1σ level. Values of $k_1(T)$, calculated from eq 13, are in reasonably close agreement with those derived from the evaluations of Baulch *et al.*[34] and Hanson and Salimian.[35] The recommended expression of Tsang and Herron[36] diverges from eq 13, and at 1200 K their value for $k_1(T)$ is about 50% lower than that derived from the composite of the ARAS data. We recommend the Arrhenius expression, eq. 13, derived from fitting the composite ARAS data set of 278 points because of the good agreement among these data and because the ARAS technique is a direct method with very high detection sensitivity for determining [O] and because it is free from the influence of secondary reactions. In contrast, the other shock tube studies employed diagnostic techniques with relatively low detection sensitivity for [N_2O]. Therefore, in their analyses, these studies required complex kinetic modeling to extract values for $k_1(T)$ and the overall stoichiometry was either not considered or an assumed value was used.

Kinetic simulations, taken together with our experimental observation that the buildup of O(^{3}P) atoms was linear over about 2 ms, clearly show that the recommended[36] overall rate constant for the O(^{3}P) + N_2O reaction is much too large. Upper limit values for k_2 were estimated from the data for seven experimental runs. Over the temperature range $1200 \leq T \leq 1400$ K, the present upper limit for k_2 is about an order of magnitude smaller than the recommended value of Tsang and Herron[36] with an uncertainty factor of about 3. This result, therefore, suggests that further work will be required to establish accurate rate constants and the branching fraction for the reaction of O(^{3}P) with N_2O.

Acknowledgment. We thank Professors W. Fujii and P. Roth and Drs. P. Frank, P. Glarborg, and J. V. Michael for providing tabulated data of their published results. This work was supported by the Chemical Sciences Division, Office of Basic Energy Sciences, U.S. Department of Energy, under Contract No. DE-AC02-76CH00016.

References and Notes

(1) (a) Johnsson, J. E.; Glarborg, P.; Dam-Johansen, K. *Proceedings of the 24th International Symposium on Combustion*; The Combustion Institute: Pittsburgh, 1992; p 917. (b) Glarborg, P; Johnsson, J. E.; Dam-Johansen, K. *Combust. Flame* **1994**, *99*, 523.

(2) Allen, M. T.; Yetter, R. A.; Dryer, F. L. *Int. J. Chem. Kinet.* **1995**, *27*, 883.

(3) Barton, S. C.; Dove, J. E. *Can. J. Chem.* **1969**, *47*, 521.

(4) Vompe, G. A. *Russ. J. Phys. Chem. (Transl. of Zh. Fiz. Khim.)* **1973**, *47*, 788.

(5) Balaknine, V. P.; Vandooren, J; Van Tiggelen, P. J. *Combust. Flame* **1977**, *28*, 165.

(6) Soloukhin, R. I. *Dokl. Phys. Chem.* **1972**, *207*, 912.

(7) Fishborne, E. S.; Edse, R. *J. Chem. Phys.* **1966**, *44*, 515.

(8) Lipkea, W. H.; Milks, D.; Matula, R. A. *Combust. Sci. Technol.* **1973**, *6*, 257.

(9) Dove, J. E.; Nip, W. S.; Teitelbaum, H. In *Proceedings of the 15th International Symposium on Combustion*; The Combustion Institute: Pittsburgh, 1975; p 903.

(10) Baber, S. C.; Dean, A. M. *Int. J. Chem. Kinet.* **1975**, *7*, 381.

(11) Jost, W.; Michel, K. W.; Troe, J.; Wagner, H. Gg. *Z. Naturforsch. A. Phys. Sci.* **1964**, *19*, 59.

(12) (a) Martinengo, A.; Troe, J.; Wagner, H. Gg. *Z. Phys. Chem. (Munich)* **1966**, *51*, 104. (b) Olschewski, H. A.; Troe, J.; Wagner, H. Gg. *Ber. Bunsen-Ges. Phys. Chem.* **1966**, *70*, 450.

(13) Borisov, A. A.; Skachkov, G. I. *Kinet. Catal. (Transl. of Kinet. Katal.)* **1972**, *13*, 42.

(14) Zaslonko, I. S.; Losev, A. S.; Mozzhukhin, E. V.; Mukoseev, Yu. K. *Kinet. Catal. (Transl. of Kinet. Katal.)* **1980**, *21*, 311.

(15) Röhrig, M.; Petersen, E. L.; Davidson, D. F.; Hanson, R. K. *Int. J. Chem. Kinet.* **1996**, *28*, 599.

(16) (a) Dean, A. M. *Int. J. Chem. Kinet.* **1976**, *8*, 459. (b) Dean, A. M.; Steiner, D. C. *J. Chem. Phys.* **1977**, *66*, 598.

(17) Hidaka, Y.; Takuma, H.; Suga, M. *Bull. Chem. Soc. Jpn.* **1985**, *58*, 2911.

(18) (a) Roth, P.; Just, Th. *Ber Bunsen-Ges. Phys. Chem.* **1977**, *81*, 572. (b) Roth, P.; Just, Th. In *Proceedings of the 20h International Symposium on Combustion*; The Combustion Institute: Pittsburgh, 1985; p 807. (c) Tabulated data received from P. Roth, personal communication.

(19) Pamidimukkala, K. M.; Lifshitz, A.; Skinner, G. B.; Wood, D. R. *J. Chem. Phys.* **1981**, *75*, 1116.

(20) (a) Frank, P.; Just, Th. *Ber. Bunsen-Ges. Phys. Chem.* **1985**, *89*, 181. (b) Tabulated data received from P. Frank, personal communication.

(21) (a) Fujii, W.; Sagawai, S.; Sato, T.; Nosaka, Y.; Miyama, H. *J. Phys. Chem.* **1989**, *93*, 5474. (b) Tabulated data received from W. Fujii, personal communication

(22) (a) Michael, J. V.; Lim, K. P. *J. Chem. Phys.* **1992**, *97*, 3228. (b) Tabulated data received from J. V. Michael, personal communication.

(23) Loirat, H.; Caralp, F.; Forst, W.; Schoenenberger, C. *J. Phys. Chem.* **1985**, *89*, 4586.

(24) Monat, J. P.; Hanson, R. K.; Kruger, C. H. *Combust. Sci. Technol.* **1977**, *16*, 21.

(25) Sulzman, K. G. P.; Kline, J. M.; Penner, S. S. In *Proceedings of the 12th International Symposium on Shock Tubes Waves*; University of Washington Press: Seattle, 1980, p 465.

(26) (a) Gilbert, R. G.; Ross, I. G. *Aust. J. Chem.* **1971**, *24*, 1541. (b) Gilbert, R. G.; Ross, I. G. *J. Chem. Phys.* **1972**, *57*, 2299.

(27) (a) Troe, J.; Wagner, H. Gg. In *Physical Chemistry of Fast Reactions*; Levitt, B. P., Ed.; Plenum Press: London; 1973; Chapter 1. (b) Dove, J. E.; Troe, J. *J. Chem. Phys.* **1978**, *35*, 1.

(28) Endo, H.; Glanzer, K.; Troe, J. *J. Phys. Chem.* **1979**, *83*, 2083.

(29) (a) Forst, W.; Penner, A. P. *J. Chem. Phys.* **1980**, *72*, 1435. (b) Forst, W. *J. Phys. Chem.* **1982**, *86*, 1771. (c) Forst, W. *J. Phys. Chem.* **1982**, *86*, 1776.

(30) Gilbert, R. G.; Smith, S. C. In *Theory of Unimolecular and Recombination Reactions*; Blackwell Scientific: Boston, 1990 and references therein.

(31) Pritchard, H. O.; Vatsya, S. R. *J. Phys. Chem.* **1992**, *96*, 172.

(32) Chang, A. H. H.; Yarkony, D. R. *J. Chem. Phys.* **1993**, *99*, 6824.

(33) Breshears, W. D. *J. Phys. Chem.* **1995**, *99*, 12529.

(34) Baulch, D. L.; Drysdale, D. D.; Horne, D. G.; Lloyd, A. C. *Evaluated Kinetic Data for High Temperature Reactions*; Butterworths: London, 1973; p 2.

(35) Hanson, R. K.; Salimian, S. In *Combustion Chemistry*; Gardiner, W. C., Jr., Ed.; Springer-Verlag: New York, 1984.

(36) Tsang, W.; Herron, J. T. *J. Phys. Chem. Ref. Data* **1991**, *20*, 609.

(37) Mallard, W. G.; Westley, F.; Herron, J. T.; Hampson, R. F. *NIST Chemical Kinetics Database* Version 6.01, NIST Standard Reference Database 17, Gaithersberg, MD, 1994.

(38) Verem'ev, E. S.; Kislykh, V. V.; Sidel'nikov, A. E. *Kinet. Catal. (Transl. of Kinet. Katal.)* **1972**, *13*, 269 (as cited in ref 37).

(39) Znev, A. P.; Starikovskii, A. Y. *Khim. Fiz.* **1991**, *10*, 52 (as cited in ref 37).

(40) Davidson, D. F.; DiRosa, A. Y.; Chang, A. Y.; Hanson, R. K. In *Proceedings of the 18th International Symposium on Shock Tubes Waves*; VCH: Weinheim, 1992; p 183.

(41) (a) Michael, J. V.; Sutherland, J. W.; Klemm, R. B. *Int. J. Chem. Kinet.* **1985**, *17*, 315. (b) Michael, J. V.; Sutherland, J. W. *Int. J. Chem. Kinet.* **1986**, *18*, 490. (c) Sutherland, J. W.; Klemm, R. B. In *Proceedings of the 16th International Symposium on Shock Tubes and Waves;* VCH: Weinheim, 1988; pp 395−402 and references therein.

(42) Sutherland, J. W.; Michael, J. V.; Klemm, R. B. *J. Phys. Chem.* **1986**, *90*, 5941.

(43) Klemm, R. B.; Sutherland, J. W.; Wickramatchi, M. A.; Yarwood, G. *J. Phys. Chem.* **1990**, *94*, 3354.

(44) (a) Sutherland, J. W.; Patterson, P. M.; Klemm, R. B. *J. Phys. Chem.* **1990**, *94*, 2471. (b) Patterson, P. M.; Sutherland, J. W.; Klemm, R. B. In *Proceedings of the 17th International Symposium on Shock Waves and Shock Tubes;* AIP: New York, 1990; pp 444−9.

(45) Yarwood, G.; Sutherland, J. W.; Wickramatchi, M. A.; Klemm, R. B. *J. Phys. Chem.* **1991**, *95*, 8771.

(46) Klemm, R. B.; Sutherland, J. W.; Rabinowitz, M. J.; Patterson, P. M.; Quartemont, J. M.; Tao, W. *J. Phys. Chem.* **1992**, *96*, 1786.

(47) (a) Myerson, A. L.; Watts, W. S. *J. Chem. Phys.* **1968**, *49*, 425. (b) Meyerson, A. L.; Thompson, H. M.; Joseph, P. J. *J. Chem. Phys.* **1965**, *42*, 3331.

(48) Bradley, J. N. *Shock Waves in Chemistry and Physics*; Wiley: New York, 1962.

(49) Greene, E. F.; Toennies, J. P. *Chemical Reactions in Shock Waves*; Academic Press: New York, 1964.

(50) Okabe, H. *Photochemistry of Small Molecules*; John Wiley & Sons, Inc.: New York; 1978; p 219.

(51) Kee, R. J.; Rupley, F. M.; Miller, J. A. CHEMKIN-II: A Fortran Chemical Kinetic Package for the Analysis of Gas-Phase Chemical Kinetics. Report SAND89−8009; Sandia National Laboratories: Albuquerque, NM, 1989.

(52) Press, W. H.; Flannery, B. P.; Teukolsky, S. A.; Vetterling, W. T. *Numerical Recipes in Pascal*; Cambridge University Press, Cambridge; 1989; p 574.